

Scalable superconducting memory with a pseudo-spin-valve barrier^a

Burm Baek, William H. Rippard, Samuel P. Benz, Stephen E. Russek, and Paul D. Dresselhaus

National Institute of Standards and Technology, 325 Broadway, Boulder, CO 80305, USA

Abstract

The quantum behavior of Josephson junctions is often exploited to produce superconducting devices of outstanding performance. With respect to information technology applications, Josephson junctions can be used in circuits that perform logic operations in picoseconds, which may result in energy-efficient, high-performance cryogenic computers, provided that memory elements can be developed that can be switched between two stable states by integrated superconducting logic circuits. Here, we show that Josephson junctions based on pseudo-spin-valve barriers could enable such memory elements, by unambiguously differentiating the controlled changes in Josephson coupling from size-dependent remanent-field effects. These changes can be very large and even reversed in magnitude, which is strong evidence of the exchange-field effect on the Cooper pair phase. These devices are the first that demonstrate nonvolatile, size-independent switching of the Josephson coupling in magnitude or phase, and they may allow for the first scalable superconducting memory devices.

Recent advances in the understanding of superconductor-ferromagnet (S-F) hybrid structures have revealed exciting physical phenomena, such as devices in which the Josephson ground-state phase difference between the two superconductors is shifted by π compared to that of conventional junctions, or in which Josephson coupling is achieved via a spin-polarized triplet state^{1,2}. Combining the

superconducting quantum and spintronic effects into low-power bi-stable devices that are switchable between different memory states could transform high-performance computing and elevate superconducting digital technology³ as a serious alternative to existing power-hungry computers based on semiconductor technology. Despite the demonstration, over a decade ago, of a ≈ 700 GHz clock-rate logic element⁴, the lack of a practical and scalable cryogenic memory is one reason that superconducting digital electronics has been implemented only in niche applications^{5,6}. Past cryogenic-memory efforts employed circuits that stored magnetic flux quanta in superconducting loops or combined Josephson and CMOS technologies in hybrid circuits^{7,8}. Unfortunately, these approaches did not simultaneously offer high-speed, ultra-low-power, and scalability.

Storing information within a Josephson junction (JJ) by changing its state is a straightforward approach to making a cryogenic memory that is both practical and scalable. One way to do this is by inserting magnetic layers within the barrier of a JJ so that the magnetic configuration changes the superconducting critical current that separates zero and nonzero voltage states. A number of magnetically controlled Josephson switches have been demonstrated. Clinton *et al.*⁹ demonstrated microbridge devices that switched between different critical currents using the stray field of a ferromagnet. More recently, critical-current switching was demonstrated by incorporating a single ferromagnetic layer into a JJ barrier¹⁰. In both devices, the difference in the critical current of the two states, or the signal contrast, comes from the magnitude and direction of the remanent magnetic field within the microbridge or the junction barrier. However, these devices will require a significant ferromagnetic moment and, thus a high magnetic switching energy at submicrometer junction dimensions, which would make them practical only for low-density memory. Scalable JJ devices should be based on direct manipulation of the Josephson coupling by use, for example, of barriers such as a pseudo-spin-valve (PSV)¹¹ or a multi-layer film structure with noncollinear magnetizations of the different layers for enhanced triplet coupling. Triplet superconductivity has recently become a subject of intense study due to the finite spin current and the long Cooper-pair coherence length in a ferromagnet^{2,12-17}. Bi-stable devices appropriate for a cryogenic

memory based on this effect have not been demonstrated, and their generally complicated multilayer structure and control of their noncollinear magnetic state may make such devices less practical than those based on a PSV. In this article, we focus on JJs based on PSV barriers.

A PSV comprises two different ferromagnetic layers separated by a nonmagnetic metal. Typically, its resistance state is changed through the giant magnetoresistance (GMR) effect by changing the orientation of the magnetization of one layer with respect to the other¹⁸. Writing information [i.e., switching the PSV state between the parallel (P) and anti-parallel (AP) magnetizations] to a typical PSV device can be accomplished either by applying a magnetic field to switch the magnetization of the layer with lower coercivity or, in nanoscale devices, by applying a bias current to switch the magnetization through the spin-transfer torque effect¹⁹. Regarding the superconducting transport properties of an S-PSV-S JJ, S-F proximity theory provides a physical understanding as well as a method for quantitative analysis^{1,2}. The exchange field in the ferromagnet splits the two electronic spin bands, resulting in a spatial phase modulation of the Cooper-pair condensate emanating from each superconductor. This effect leads to oscillating decay, including sign reversal, of the Josephson coupling as a function of the magnetic barrier thickness. By placing a second F layer in the barrier, the total phase shift may be increased or decreased, depending on the relative orientations of the magnetizations of the F layers (i.e., P or AP), and this may produce a corresponding change in the critical current of the junction.

Experimental studies of JJs with double magnetic barriers of collinear magnetizations were carried out by Bell *et al.*¹¹ and later by Robinson *et al.*²⁰ with S-PSV-S and S-F-N-F-S (N: nonmagnetic and nonsuperconducting metal) JJs, respectively. In both studies, enhanced maximum supercurrents were observed for the AP states compared with the P states. Both works concluded that their results were due to the exchange-field effect on the pair phase, based on an argument that the phase shift in the AP state was smaller than in the P state and produced a larger, less modulated critical current. However, the interpretation of these results is complicated by competing effects. In such structures, a remanent field from the magnetic barrier induces a non-uniform supercurrent distribution within the junction and results

in a maximum total supercurrent I_m that is reduced from the critical current $I_c \equiv J_c A$, given by critical current density J_c and the junction area A ^{21,22}. Regarding the two experiments quoted above, the higher I_m in the AP state may be attributed to the lower average remanent field, as compared to that of the P state. For a rectangular junction with uniform distributions of magnetic field and J_c distributions in the barrier, I_m decays with increasing magnetic flux Φ in an oscillating fashion where $I_m = I_c |\sin(\pi\Phi/\Phi_0)|/(\pi\Phi/\Phi_0)$ (known as a Fraunhofer pattern^{21,22}). Here, Φ_0 is the magnetic flux quantum. Thus, in order to fully characterize the state of such a junction, we must extract the I_c , which is the maximum supercurrent at zero net flux in the barrier (not at zero applied field), determined from the maximum value of $I_m(H)$, where H is the applied magnetic field.

In this work, we performed detailed $I_m(H)$ and other measurements to clearly discriminate between remanent-field effects and the more direct exchange-field effect on Josephson coupling. Distinguishing these two effects is key to understanding the physics governing these devices and evaluating their scaling potential. We found that the material choices were crucial in obtaining unambiguous results. The PSV must include materials with different coercivities, so that the device can be placed into both the P and AP states. Weaker ferromagnets make the oscillation and decay length of the Cooper pair longer and enable the use of thicker films, which is advantageous for the reproducibility of the devices. However, the free-layer coercivity must be high enough to show a large portion, including the peak, of the main lobe of the Fraunhofer pattern associated with each magnetic state of the PSV.

We used Ni as the higher-coercivity layer, since its saturation magnetization is relatively low, and at 10 K its measured coercivity is ≈ 40 mT, which is adequate for a PSV hard layer. For the free layer, we chose $\text{Ni}_{0.7}\text{Fe}_{0.17}\text{Nb}_{0.13}$, which had a coercivity of ≈ 2 mT at 10 K and a reduced magnetic moment with Nb doping²³ (Fig. 1 inset). The S-PSV-S multilayer films were sputter-deposited on oxidized silicon wafers in a chamber without breaking vacuum. Each device had the following film deposition sequence and thicknesses: Nb(100 nm)/Cu(3 nm)/ $\text{Ni}_{0.7}\text{Fe}_{0.17}\text{Nb}_{0.13}(d_{\text{NiFeNb}})$ /Cu(5 nm)/Ni(d_{Ni})/Cu(3 nm)/Nb(70 nm). The $\text{Ni}_{0.7}\text{Fe}_{0.17}\text{Nb}_{0.13}$ layers were grown by co-sputtering $\text{Ni}_{0.8}\text{Fe}_{0.2}$ and Nb targets. The Cu layers adjacent

to each Nb layer serve as buffers or growth templates for the ferromagnetic layers and are expected to be superconducting due to the proximity effect at 4 K. The center spacer Cu layer prevents exchange coupling and reduces magnetostatic coupling between the $\text{Ni}_{0.7}\text{Fe}_{0.17}\text{Nb}_{0.13}$ and the Ni, allowing them to switch independently. Using a superconducting quantum interference device (SQUID) magnetometer, we measured the Nb superconducting temperature $T_c \approx 8.9$ K and observed hysteretic magnetization loops with two well-separated switching fields in the unpatterned multilayers (Fig. 1).

Four-point electrical measurements were used to characterize JJs with different dimensions and barrier materials. Wafers of test chips containing these junctions were fabricated with reliable, high-throughput processes, employing stepper lithography and reactive ion etching. The barrier etching was done by ion milling monitored with an ion mass spectrometer. The rest of the fabrication process is similar to that used to fabricate NIST Josephson voltage standards²⁴. There was no noticeable deleterious change in the magnetic properties of the films due to the device processing. For junctions with designed dimensions less than 2 μm , the actual fabricated feature dimensions were significantly smaller due to process runout. For example, the smallest junctions studied were elliptical, with the short and long axes of 0.9 μm and 1.8 μm by design, but yielded effective areas $A_{\text{eff}} \approx 0.5 \mu\text{m}^2$ according to their measured resistances.

We conducted most of the electrical measurements in a liquid-helium bath at 4 K, using a dipping probe with a superconducting magnet. A magnetic field was applied parallel to the long axes of the devices. The current-voltage (I - V) characteristics at each magnetic field were fit to the resistively-shunted junction model²¹, yielding I_m and the normal resistance R_n (Fig. 2c). Due to the GMR effect, the junction resistance is slightly smaller in the P state than in the AP state. The magnetoresistance ratio is roughly 0.2 % in a $\text{Ni}_{0.7}\text{Fe}_{0.17}\text{Nb}_{0.13}$ (2 nm)-Ni(3 nm) PSV.

Fig. 2a shows the measured $I_m(H)$ of an S-F-S JJ (an S-PSV-S junction with an ultrathin Ni layer thickness, $d_{\text{Ni}} < 0.1$ nm) with the magnetic field swept in both directions in order to see the magnetic

hysteresis. For this control sample, the Ni is so thin that it has no measureable moment and the barrier is effectively a single magnetic layer. From the positive field limit to roughly -5 mT, the magnetic state of the device stays close to a fully-magnetized, single-domain state, and the $I_m(H)$ characteristic follows a smooth Fraunhofer-like pattern. Excluding the abrupt changes, where the $\text{Ni}_{0.7}\text{Fe}_{0.17}\text{Nb}_{0.13}$ layer switches, these data can be fit by conventional theory with a horizontal shift to account for the offsets due to the net self-field of the ferromagnetic state within the barrier. We use for a perfect circular or elliptical junction²¹, $I_m = I_c |2J_1(\pi\Phi/\Phi_0)|/(\pi\Phi/\Phi_0)$, where J_1 is a Bessel function of the first kind, to fit our data. Since $I_m(H)$ is sensitive to junction shape, J_c uniformity, field uniformity, etc., this simple formula is not expected to provide a perfect fit at high fields. However, it works reasonably well for the main lobes of both PSV states. Such undistorted shapes as well as the nodes with $I_m \approx 0$ indicate no trapped flux in the junction. Each pattern is shifted in the direction opposite to the $\text{Ni}_{0.7}\text{Fe}_{0.17}\text{Nb}_{0.13}$ magnetization, as expected. The critical current I_c for each magnetization state is defined by the main peak of each $I_m(H)$ for that state. The critical currents for each state are identical for this S-F-S junction, indicating no change in the Josephson coupling (I_c or J_c), because the magnetization of the single F layer in the barrier is simply changing direction.

When adding a thicker Ni layer to form a PSV barrier, we find a different I_c for each magnetic state of the S-PSV-S junction (Fig. 2b). We magnetized the Ni layer to near-saturation with $\mu_0 H \approx 200$ mT and removed the resulting trapped flux in the superconducting Nb by raising the sample temperature above 9 K. The sample temperature was then lowered to 4 K and I_m was measured over a ± 10 mT field range. The abrupt transitions of $I_m(H)$ indicate that the reversal of the $\text{Ni}_{0.7}\text{Fe}_{0.17}\text{Nb}_{0.13}$ layer begins at -4 mT in one direction and at +3 mT in the other direction. The two distinctly different peak values, $I_c^P = 0.11$ mA and $I_c^{AP} = 0.07$ mA for P and AP states, respectively, definitively demonstrate that the Josephson coupling can be controllably modulated by the exchange field in a PSV and that our measurements have successfully differentiated the Josephson coupling from the remanent-field effect. The remanent-field effect is significant for junction areas down to $\approx 1 \mu\text{m}^2$ in our devices, despite the use of weak and thin

ferromagnets. However, any nanoscale device designed to exploit the remanent-field effect will suffer from a small I_m modulation, because a reduced total magnetic moment and an increased demagnetizing field in the barrier result in a smaller magnetic flux trapped in the junction. The change in I_c , $\Delta I_c \equiv I_c^P - I_c^{AP}$, by the exchange field persists in our smallest junctions as well as in the largest ones (Fig. 3a). These results, for the first time, demonstrate the possibility of switchable nanoscale superconducting devices that may enable high-density integration for practical cryogenic memory.

Analysis of junctions with a range of d_{Ni} and A_{eff} provides further insight into the exchange-field effect in S-PSV-S devices. The results presented in Figs. 2b, 3a, and 3b show that $I_c^P < I_c^{AP}$, or $\Delta I_c < 0$. Since the exchange-field effect produces a phase shift of the pair wavefunction, if the thickness of one of the F layers is varied, then ΔI_c will oscillate as well, including sign changes. That is, the slope of a sinusoidal function oscillates as well as the function itself. Figs. 3e and 3f illustrate this point with the PSV barrier structure projected to a single F, that adds a phase proportional to an effective F thickness; here, we do not take account of the phase decoherence that leads to a decay in I_c . The phase shift, hence the effective F thickness, is larger for the P state than for the AP state and, depending on the slope at the effective thickness of the hard layer (black dashed lines), the sign of ΔI_c can be either positive or negative. We demonstrated this behavior by fabricating and measuring JJs with different Ni thicknesses in the PSV barrier. As shown in Figs. 3c and 3d, we found two Ni thicknesses, $d_{Ni} = 1.5$ nm and 2.0 nm, that produced very large ΔI_c with opposite signs. Such a sign change in ΔI_c is a signature of the exchange-field effect, which has not been observed to date. A more complete trend has been obtained by varying d_{Ni} . With $0 < d_{Ni} < 4$ nm, we obtained a characteristic voltage $V_c \equiv I_c R_n$, for each state, V_c^P and V_c^{AP} , which showed different oscillatory trends (Fig. 4). We can readily understand that ΔV_c also oscillates and changes sign. Each $V_c(d_{Ni})$ has a typical trend observed in S-F-S JJs^{25,26} with different offsets in d_{Ni} between the P and the AP states. Such different thickness offsets, d_o^P and d_o^{AP} , originate from the added opposite phases with the two different magnetization orientations of the $Ni_{0.7}Fe_{0.17}Nb_{0.13}$ layer.

Consequently, both V_c^P and V_c^{AP} can be described by an S-F-S theory for the clean limit with different d_o^P and d_o^{AP} , respectively²⁷:

$$V_c = \frac{\pi\Delta^2}{4eT} \int_{\alpha}^{\infty} \frac{dy}{y^3} \alpha^2 \cos y. \quad (1)$$

In (1), Δ is the order parameter of the superconducting electrodes, T is the temperature, and $\alpha \equiv 2E_{\text{ex}}[d_{\text{Ni}} - d_o]/\hbar v_F$ with the exchange energy E_{ex} of Ni and the Fermi velocity v_F . The use of this quasiclassical theory should be appropriate for Ni thicknesses between several atomic layers and the electron mean free path (e.g., ~ 5 nm from Blum *et al.*²⁸) and results in good fits to the measured V_c data for $d_{\text{Ni}} \geq 1.5$ nm (see Fig. 4). d_o includes the thin effective dead layer d_{dead} in Ni; we obtained $d_{\text{dead}} = (d_o^P + d_o^{AP})/2 \approx 0.8$ nm, i.e., a dead layer of 0.4 nm at each Ni/Cu interface. This is comparable to the commonly observed magnetic dead layers in F/N structures²⁹ and roughly consistent with our measured saturation magnetization *vs.* thickness of Ni without a $\text{Ni}_{0.7}\text{Fe}_{0.17}\text{Nb}_{0.13}$ layer. We expect a non-oscillatory decay of V_c and zero ΔV_c within the dead layer if the ferromagnetism is completely suppressed^{30,31}. However, the exchange-field effect, and hence nonzero ΔV_c , may gradually appear around d_{dead} . The V_c (or J_c) oscillating period of 2.6 nm and the characteristic length given by $\hbar v_F/2E_{\text{ex}} = 1$ nm roughly agree with past reports regarding simple Nb/Ni/Nb JJs^{28,30,31}.

Possibilities of new device applications follow from this exchange-field effect. The node in each $V_c(d_{\text{Ni}})$ in Fig. 4 represents the transition of the zero-field JJ ground state from 0 to π in phase difference^{1,2,25,26}. Such transitions occur at different d_{Ni} values of 1.6 nm and 2.1 nm for the P and AP states, respectively, which implies that JJs with $1.6 \text{ nm} < d_{\text{Ni}} < 2.1 \text{ nm}$ are phase-switchable devices. Phase-shifting elements are novel components of superconducting digital and qubit electronics³²⁻³⁵. Among the different device types, S-F-S JJs are often considered the most promising architecture for a π -phase-shifter due to their nonvolatility and small size³⁵. For example, the proposed elimination of the superconducting loops in some rapid single-flux quantum logic components by use of π -JJs³³ has been

experimentally demonstrated with S-F-S devices³⁶. It will be interesting to see what kind of novel future electronics will be conceived and realized with the added capability of *in situ*, nonvolatile phase-switching offered by S-PSV-S JJs. Regarding the cryogenic memory application of these devices, the near-extinction of I_c at a $0-\pi$ transition is an important feature, since it facilitates reliable discrimination of the information stored in the PSV states. A large bias-current margin for discriminating between the low and high I_c states in a cryogenic memory based on single JJs will be essential in overcoming device-parameter spreads in highly-integrated circuits. A useful metric for this margin is the relative change in I_c , $|\Delta I_c|/(\text{the lesser of } I_c^P \text{ and } I_c^{AP}) \approx 500\%$ for $d_{\text{Ni}} = 1.5$ nm (Fig. 3c). This is well beyond a typical GMR ratio of a spin valve ($< 10\%$)¹⁸ and comparable to the best present-day tunneling magnetoresistance (TMR) ratios of $\approx 600\%$ at room temperature and $\approx 1100\%$ at 4.2 K³⁷. Determining the fundamental limit to that margin may require investigation of higher-harmonic Josephson currents^{27,30,38}.

The exchange field behavior that we distinguished from the remanent-field effects remains size independent in this work. However, further research on smaller nanoscale devices is needed to determine the scalability limits of these devices. More efficient magnetization switching with spin-transfer torque may be effective in nanoscale PSVs. The results in this paper demonstrate that Josephson junctions with pseudo-spin-valve barriers have the potential to enable low-power, high-speed, high-density cryogenic memory for a high-performance superconducting computing system.

Acknowledgements

The authors thank M. R. Pufall and H. Rogalla for technical assistance and valuable discussions. This work was supported by NIST and by U.S. National Security Agency under agreement numbers EAO156513 and EAO176792.

- a. Work of the U. S. government, not subject to U. S. copyright.

References

1. Buzdin, A. I. Proximity effects in superconductor/ferromagnet heterostructures. *Rev. Mod. Phys.* **77**, 935976 (2005).
2. Bergeret, F. S., Volkov, A. F. & Efetov, K. B. Odd triplet superconductivity and related phenomena in superconductor-ferromagnet structures. *Rev. Mod. Phys.* **77**, 1321–1373 (2005).
3. Likharev, K. K. & Semenov, V. K. RSFQ logic/memory family: A new Josephson-junction technology for sub-terahertz-clock-frequency digital systems. *IEEE Trans. Appl. Supercond.* **1**, 328 (1991).
4. Chen, W., Rylyakov, A. V., Patel, V., Lukens, J. E. & Likharev, K. K. Superconductor digital frequency divider operating up to 750 GHz. *Appl. Phys. Lett.* **73**, 2817–2819 (1998).
5. Bedard, F., Welker, N., Cotter, G. R., Escavage, M. A. & Pinkston, J. T. Superconducting technology assessment. (Nat. Security Agency Office Corp. Assessments, Fort Meade, MD, USA, 2005).
6. Holmes, D. S., Ripple, A. L. & Manheimer, M. A. Energy-Efficient Superconducting Computing—Power Budgets and Requirements. *IEEE Trans. Appl. Supercond.* **23**, 1701610 (2013).
7. Nagasawa, S., Hashimoto, Y., Numata, H. & Tahara, S. A 380 ps, 9.5 mW Josephson 4-Kbit RAM operated at a high bit yield. *IEEE Trans. Appl. Supercond.* **5**, 2447–2452 (1995).
8. Van Duzer, T., Zheng, L., Whiteley, S. R., Kim, H., Kim, J., Meng, X. & Ortlepp, T. 64-kb Hybrid Josephson-CMOS 4 Kelvin RAM With 400 ps Access Time and 12 mW Read Power. *IEEE Trans. Appl. Supercond.* **23**, 1700504 (2013).
9. Clinton, T. W. & Johnson, M. Nonvolatile switchable Josephson junctions. *J. Appl. Phys.* **85**, 1637-1643 (1999).

10. Larkin, T., Bol'ginov, V., Stolyarov, V., Ryazanov, V., Vernik, I., Tolpygo, S. & Mukhanov, O. Ferromagnetic Josephson switching device with high characteristic voltage. *Appl. Phys. Lett.* **100**, 222601 (2012).
11. Bell, C., Burnell, G., Leung, C. W., Tarte, E. J. Kang, D. J. & Blamire, M. G. Controllable Josephson current through a pseudospin-valve structure. *Appl. Phys. Lett.* **84**, 1153 (2004).
12. Keizer, R. S., Goennenwein, S. T. B., Klapwijk, T. M., Miao, G. X., Xiao, G. & Gupta, A. A spin triplet supercurrent through the half-metallic ferromagnet CrO₂. *Nature* **439**, 825–827 (2006).
13. Eschrig, M. & L fwander, T. Triplet supercurrents in clean and disordered half-metallic ferromagnets. *Nature Phys.* **4**, 138–143 (2008).
14. Robinson, J. W. A., Witt, J. D. S. & Blamire, M. G. Controlled Injection of Spin-Triplet Supercurrents into a Strong Ferromagnet. *Science* **329**, 59–61 (2010).
15. Khaire, T. S., Khasawneh, M. A., Pratt, W. P., Jr. & Birge, N. O. Observation of Spin-Triplet Superconductivity in Co-Based Josephson Junctions. *Phys. Rev. Lett.* **104**, 137002 (2010).
16. Klose, C. et al. Optimization of Spin-Triplet Supercurrent in Ferromagnetic Josephson Junctions. *Phys. Rev. Lett.* **108**, 127002 (2012).
17. Leksin, P. V., Garif'yanov, N. N., Garifullin, I. A., Fominov, Y. V., Schumann, J., Krupskaya, Y., Kataev, V., Schmidt, O. G. & Bu chner, B. Evidence for Triplet Superconductivity in a Superconductor-Ferromagnet Spin Valve. *Phys. Rev. Lett.* **109**, 057005 (2012).
18. Wolf, S. A. et al. Spintronics: A Spin-Based Electronics Vision for the Future *Science*. **294**, 1488–1495 (2001).
19. Slonczewski, J. C. Current-driven excitation of magnetic multilayers. *J. Magn. Magn. Mater.* **159**, L1 (1996).
20. Robinson, J. W. A., Halasz, G. B., Buzdin, A. I. & Blamire, M. G. Enhanced Supercurrents in Josephson Junctions Containing Nonparallel Ferromagnetic Domains. *Phys. Rev. Lett.* **104**, 207001 (2010).
21. Tinkham, M. Introduction to Superconductivity (McGraw-Hill, New York, 1975).

22. Likharev, K. K. Dynamics of Josephson Junctions & Circuits (Gordon & Breach Science Publishers, New York, 1986).
23. Chen, M.-M., Gharsallah, N., Gorman, G. L. & Latimer, J. Ternary NiFeX as soft biasing film in a magnetoresistive sensor. *J. Appl. Phys.* **69**, 5631–5633, (1991).
24. Chong, Y., Burroughs, C. J., Dresselhaus, P. D., Hadacek, N., Yamamori, H. & Benz, S. P. Practical high-resolution programmable Josephson voltage standards using double- and triple-stacked MoSi-barrier junctions. *IEEE Trans. Appl. Supercond.* **15**, 461–464, (2004).
25. Kontos, T. et al. Josephson junction through a thin ferromagnetic layer: Negative coupling. *Phys. Rev. Lett.* **89**, 137007 (2002).
26. Oboznov, V. A., Bolginov, V. V., Feofanov, A. K., Ryazanov, V. V. & Buzdin, A. I. Thickness dependence of the Josephson ground states of superconductor/ferromagnet/superconductor junctions. *Phys. Rev. Lett.* **96**, 197003 (2006).
27. Buzdin, A. I., Bulaevskij, L. N. & Panyukov, S. V. Critical-current oscillations as a function of the exchange field and thickness of the ferromagnetic metal (F) in an S-F-S Josephson junction. *J. Exp. Theor. Phys. Lett.* **35**, 178–180 (1982).
28. Blum, Y., Tsukernik, A., Karpovski, M. & Palevski, A. Oscillations of the superconducting critical current in Nb-Cu-Ni-Cu-Nb junctions. *Phys. Rev. Lett.* **89**, 187004 (2002).
29. Speriosu, V. S. et al. Role of interfacial mixing in giant magnetoresistance. *Phys. Rev. B* **47**, 11579–11582 (1993).
30. Robinson, J. W. A, Piano, S., Burnell, G., Bell, C. & Blamire, M. G. Zero to Pi transition in superconductor-ferromagnet-superconductor junctions. *Phys. Rev. B* **76**, 094522 (2007).
31. Bannykh, A. A. et al. Josephson tunnel junctions with a strong ferromagnetic interlayer. *Phys. Rev. B* **79**, 054501 (2009).
32. Majer, J. B., Butcher, J. R. & Mooij, J. E. Simple phase bias for superconducting circuits. *Appl. Phys. Lett.* **80**, 36383640 (2002).

33. Ustinov, A. V. & Kaplunenko, V. K. Rapid single-flux quantum logic using π -shifters, *J. Appl. Phys.* **94**, 5405-5407 (2003).
34. Plantenberg, J. H., de Groot, P. C., Harmans, C.J.P.M. & Mooij, J. E. Demonstration of controlled-not quantum gates on a pair of superconducting quantum bits. *Nature* **447**, 836–839 (2007).
35. Mielke, O., Orllepp, Th., Dimov, B. & Uhlmann, F. H. Phase engineering techniques in superconducting quantum electronics. *J. Phys.: Conf. Ser.* **97**, 012196 (2008).
36. Feofanov, A. K. et al. Implementation of superconductor/ferromagnet/superconductor π -shifters in superconducting digital and quantum circuits *Nature Phys.* **6**, 593–597 (2010).
37. Ikeda, S. et al. Tunnel magnetoresistance of 604% at 300 K by suppression of Ta diffusion in CoFeB/MgO/CoFeB pseudo-spin-valves annealed at high temperature. *Appl. Phys. Lett.* **93**, 082508 (2008).
38. Konschelle, F., Cayssol, J. & Buzdin, A. I. Nonsinusoidal current-phase relation in strongly ferromagnetic and moderately disordered SFS junctions. *Phys. Rev. B* **78**, 134505 (2008).

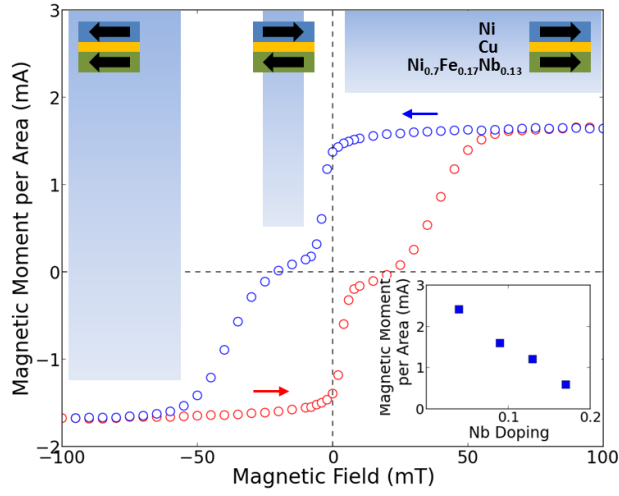


Figure 1. Hysteretic magnetization data at 10 K from an unpatterned PSV multilayer structure: Nb(100 nm)/Cu(3 nm)/Ni_{0.7}Fe_{0.17}Nb_{0.13}(2.1 nm)/Cu(5 nm)/Ni(3 nm)/Cu(3 nm)/Nb(70 nm). The field was swept from positive to negative (blue circles), then back to positive (red circles), as indicated by the colored arrows. Illustrated above the plot are the different magnetization states of the Ni and Ni_{0.7}Fe_{0.17}Nb_{0.13} for the trace with the blue circles. Inset: Trend of Ni_{0.7}Fe_{0.17}Nb_{0.13} saturation magnetization with Nb doping.

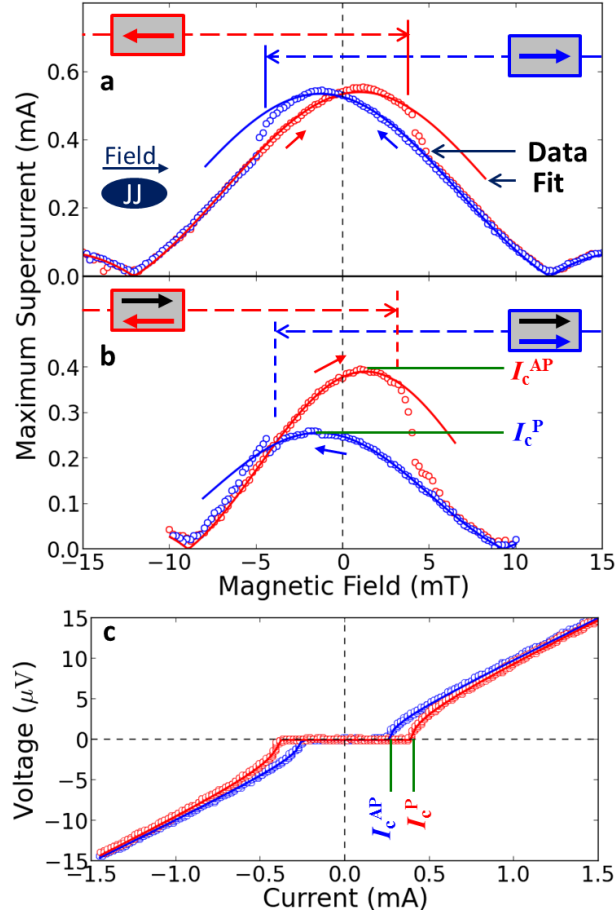


Figure 2. Electrical measurement results of S-PSV-S JJs at 4 K. **a**, Maximum supercurrent *vs.* magnetic field of a JJ with zero Ni thickness ($d_{\text{Ni}} \approx 0$) in the PSV barrier structure, $\text{Ni}_{0.7}\text{Fe}_{0.17}\text{Nb}_{0.13}(2.1 \text{ nm})/\text{Cu}(5 \text{ nm})/\text{Ni}(d_{\text{Ni}})$. The JJ design is a $0.9 \mu\text{m} \times 1.8 \mu\text{m}$ ellipse and the magnetic field is applied along the long axis of the ellipse (inset). **b**, Maximum supercurrent *vs.* magnetic field of the S-PSV-S device with $d_{\text{Ni}} = 1 \text{ nm}$. The JJ design is a $1.2 \mu\text{m} \times 2.4 \mu\text{m}$ ellipse. **c**, Current *vs.* voltage of the device used in **b** measured at the magnetic field giving in the peak I_m for each state. Symbols are measured data and lines are fits. The magnetization states are labeled by colored and black arrows in the illustrated boxes above the plots for the $\text{Ni}_{0.7}\text{Fe}_{0.17}\text{Nb}_{0.13}$ and the Ni layers, respectively.

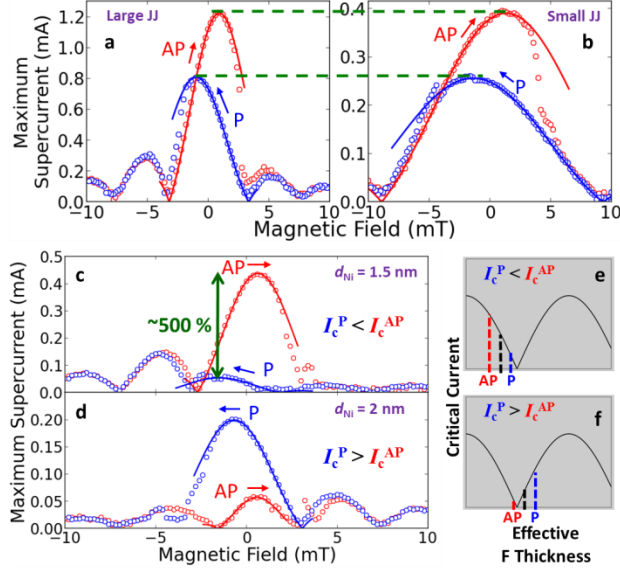


Figure 3. Maximum supercurrent vs. magnetic field characteristics of S-PSV-S JJs at 4 K with different areas and Ni thicknesses. **a** and **b** show the effects of different junction areas. The actual areas are estimated to be **a**, $2.6 \mu\text{m}^2$ and **b**, $0.78 \mu\text{m}^2$, based on the $R_{\text{N}}A_{\text{eff}} \approx 8.0 \text{ m}\Omega \mu\text{m}^2$. The JJ designs are **a**, $1.6 \mu\text{m} \times 3.2 \mu\text{m}$ and **b**, $1.2 \mu\text{m} \times 2.4 \mu\text{m}$ ellipses. The Ni thickness is 1 nm for both JJs. **c** and **d** show very large ΔI_c and with opposite signs for two different Ni thicknesses **c**, 1.5 nm and **d**, 2 nm. As designed, both JJs are $1.4 \mu\text{m} \times 2.8 \mu\text{m}$ ellipses. The symbols and the curves represent data and fits, respectively. **e-f**, Illustrations of the origin of the different ΔI_c in **c** and **d**, respectively. Effective F thickness means the Ni thickness that would result in the same phase shift in the PSV. The decay in I_c is ignored for simplicity. A P or AP state results in an increased or decreased phase (blue or red dashed line) relative to that given by the Ni thickness only (black dashed lines).

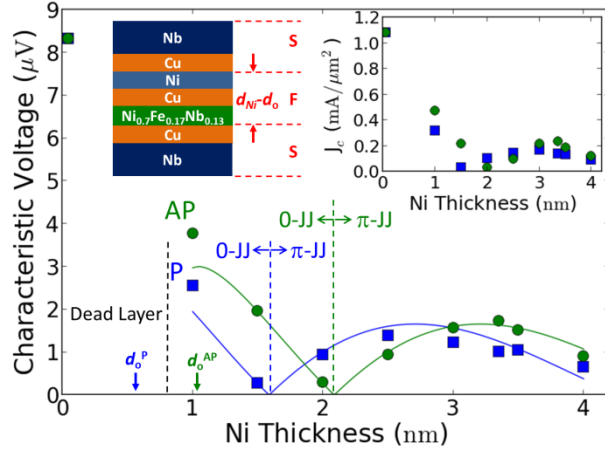


Figure 4. Characteristic voltage V_c vs. Ni thickness data (symbols) and fit (solid line) in the S–PSV–S devices with the PSV structure $\text{Ni}_{0.7}\text{Fe}_{0.17}\text{Nb}_{0.13}(2.1 \text{ nm})/\text{Cu}(5 \text{ nm})/\text{Ni}(d_{\text{Ni}})$ at 4 K. P and AP states are indicated by blue squares and green circles, respectively. Each V_c datum is an average for a few JJ samples. For $d_{\text{Ni}} < 3 \text{ nm}$, each V_c datum is an average for either 3 or 4 devices, resulting in an error bar comparable to or smaller than the maker size (the standard error of the mean $I_c \leq 20 \%$ of the mean I_c). For $d_{\text{Ni}} \geq 3 \text{ nm}$, the sample size is 1. Left inset: device multilayer structure and its equivalent S-F-S structure as an approximation. Right inset: critical current density J_c (given by $V_c/R_{\text{N}}A_{\text{eff}}$) vs. Ni thickness.